High-pressure Raman study of the charge ordering in α-$(BEDT\text{-}TTF)_2I_3$

Roman Wojciechowski,* Kaoru Yamamoto, and Kyuya Yakushi
Institute for Molecular Science, Myodaiji, Okazaki, Aichi 444-8585, Japan

Makoto Inokuchi
Department of Materials Science and Environmental Engineering, Science University of Tokyo, Yamaguchi Daigakudori, Onoda, Yamaguchi 756-0884, Japan

Atsushi Kawamoto
Department of Physics, Hokkaido University, Kita-Ku, Sapporo 060-810, Japan

(Received 12 December 2002; revised manuscript received 18 February 2003; published 16 June 2003)

Charge distributions in the donor layer for the paramagnetic semimetal-like and nonmagnetic insulating phases of the α-$(BEDT\text{-}TTF)_2I_3$ single crystal [BEDT-TTF: bis(ethylenedithiolo)tetrathiafulvalene] were investigated under quasihydrostatic pressures up to 3.6 GPa using Raman spectroscopy. The results confirmed the appearance of charge disproportionation below the metal-insulator phase transition temperature (T_{MI}). The average charge-disproportionation ratio, 0.2–0.8, at ambient pressure was quite pressure sensitive and decreased by ca. $0.1e$/GPa with increasing pressure. This result is ascribed to the faster increase of the transfer integrals than the intersite Coulomb repulsions under pressure. The loss of the inversion centers in the nonmagnetic insulating phase, concluded by the selection rule, suggests that the charge is ordered such that it forms a so-called horizontal stripe. Nonuniform charge distributions were also found at temperatures above T_{MI} for the paramagnetic semimetal-like phase. The experimentally determined small charge difference among BEDT-TTF at crystallographically nonequivalent sites is consistent with the band calculations.

DOI: 10.1103/PhysRevB.67.224105 PACS number(s): 78.30.−j, 71.30.+h

I. INTRODUCTION

In the well-known family of the $(BEDT\text{-}TTF)_2I_3$ salts[1,2] [BEDT-TTF: bis(ethylenedithiolo) tetrathiafulvalene, hereafter abbreviated as ET], four main crystal phases exist; three of these phases, i.e., β, θ, and κ, are metallic and undergo a superconducting phase transition,[3,4,5] whereas the α phase exhibits a first-order metal-insulator (MI) phase transition at $T_{MI}=135$ K.[6] The structure of α-$(ET)_2I_3$ consists of alternating anion and donor layers. At temperatures above T_{MI}, the unit cell with the $P\bar{1}$ space group accommodates four ET's; two ET's; **A** and **A′**, are combined by an inversion center and form stack I, while **B** and **C**, located on the inversion centers, form stack II [see Fig. 1(a)].[6] The band calculation predicts a two-dimensional semimetal with small electron and hole pockets.[7] Various studies have been conducted to elucidate the origin of this phase transition. Previously, Endres *et al.*,[8] Emge *et al.*,[9] and Nogami *et al.*[10] studied the low-temperature structure below T_{MI} from the structural point of view. The former two groups solved the structure with $P\bar{1}$ and found no significant structural change, with the exception of a small rotation ($\sim 1°$) of molecule **B** along the direction increasing the dihedral angle between **A** and **B**. On the other hand, the latter group suggested that the inversion symmetry was broken: that is, they proposed a weak dimerization of ET's at the **B** and **C** sites and a nonequivalence between **A** and **A′**. The low-temperature infrared spectra also suggested the breaking of inversion symmetry.[11,12] The unit cell shows a contraction along the *a* axis and expansion along the *b* axis, with a small expansion of the cell volume during the transformation to the insulating phase.[13] The paramagnetic (PM) susceptibility in the semimetal-like state gradually falls off toward T_{MI} and abruptly drops at T_{MI}. Therefore, the ground state is a nonmagnetic insulating (NI) state with a small spin gap.[14,15] The absorption spectrum in the microwave and millimeter-wave regions shows no indication of a density-wave ground state that originates from the Fermi-surface instability.[16] A calorimetric study has suggested a purely electronic nature for this phase transition, since the magnitude of the entropy change is comparable to the phase transition from a metal to an antiferromagnetic insulator in quasi-one-dimensional conductors.[13,17] Based on this finding, Heidmann *et al.* proposed a possible rearrangement of the charge distribution at temperatures below T_{MI}. However, the precision of the x-ray diffraction experiments mentioned above was insufficient to verify the charge localization that leads to the rearrangement in the charge distribution. More quantitative consideration of

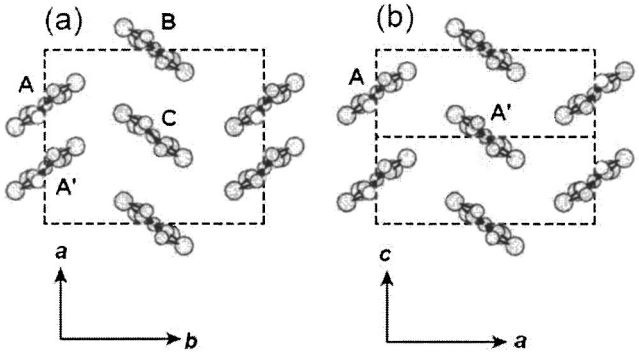

FIG. 1. Schematic representation of the structures in the donor layer of (a) α-$(ET)_2I_3$ and (b) θ-$(ET)_2I_3$.

the charge localization has been conducted based on the infrared spectrum of a powdered sample.[18] However, the infrared-active modes are screened by the strong electronic absorption and therefore there remains some ambiguity as regards the assignment of the infrared-active bands. Kino and Fukuyama theoretically investigated the MI transition of α-$(ET)_2I_3$ using mean-field theory and found that the on-site Coulomb energy U opened a gap between the third and fourth energy bands, along with the disproportionation of charge.[19,20] According to their calculations, the localized positive charge is ordered such that it forms a vertical stripe along the stack I (**A** and **A**′) with an antiferromagnetic configuration. They attributed the nonmagnetic ground state to the formation of a spin singlet in dimerized stack I (**A** and **A**′). Seo introduced intersite Coulomb interaction V and found that a vertical stripe along stack II, a vertical stripe along stack I, and a horizontal stripe became stable upon an increase in the magnitude of V/U.[21] Analyzing the magnetic susceptibility below T_{MI}, Seo proposed that the horizontal stripe would be realized in α-$(ET)_2I_3$. A recent solid-state ^{13}C NMR study supports the localization of charge and charge disproportionation at temperatures below T_{MI}.[22,23] All of these studies suggest that charge ordering (CO) is a plausible explanation for this electronic phase transition. However, the rearrangement of the charge distribution in the unit cell has not been well elucidated. Recently, Yamamoto *et al.* investigated the phase transition of θ-$(ET)_2RbZn(SCN)_4$ and demonstrated that infrared and Raman experiments can verify the presence of CO.[24] This idea was based on the fact that the frequencies of some normal modes are sensitive to the molecular charge.[25,26,27] When charge disproportionation takes place, the charge-sensitive Raman bands tend to split. The analysis of these split bands gives semiquantitative evaluation of the charge-disproportionation ratio and the formation of the particular CO stripe pattern. In this study, we applied the same method to clarify the nature of the MI phase transition of α-ET_2I_3. The MI phase transition is suppressed by hydrostatic pressures above 1.5 GPa,[28,29,30] and the high-pressure PM phase shows unusual transport properties.[30] The PM and NI phases have not been studied under high pressure, except for in magnetic[14] and transport[28,29,30] experiments. This is the first spectroscopic study to examine α-ET_2I_3 under high-pressure conditions. More generally, interest in the CO state in organic charge-transfer salts is quickly growing, as the theoretical studies have thus far suggested a relationship between the charge fluctuation and pairing mechanism in superconductivity.[31,32] In this context, it is worth noting that superconductivity has been found in α-$(ET)_2I_3$ at temperatures below 7 K under a moderate uniaxial strain along the a axis.[33]

In Sec. III, we show the temperature dependence of the Raman spectrum acquired at ambient and quasihydrostatic pressures. Special attention is devoted to the spectral change at the MI phase transition. In Sec. IV, the pressure dependence of the charge-disproportionation ratio above and below the phase transition temperature is discussed. Subsequently, the type of the charge stripes is discussed.

II. EXPERIMENT

Single crystals of α-$(ET)_2I_3$ were prepared according to the reported procedure for ''natural'' ET as well as for ET labeled with ^{13}C isotope.[34] The ^{13}C was substituted only in the central C═C [hereafter referred to as $^{13}C(2)$-ET].[35] Single crystals of θ-$(ET)_2I_3$ were occasionally found in the same batch. The structure types and the directions of the a and b axes were identified by infrared (IR) reflectance spectra with the use of a Fourier transform (FT) IR spectrometer Nicolet Magna 760 combined with an IR microscope IR-Plan.[36] The crystals were mounted by grease on a cupper cold stage in a cryostat Oxford CF1104, and then they were cooled at the rate of 1.5 K/min. The cooling rate was reduced to 0.5 K/min near T_{MI}. The temperature was controlled with two silicon-diode sensors fixed to the cold stage. Raman spectra were collected in backscattering geometry using a Renishaw Ramanscope System 1000 composed of a notch filter, single monochromator, and a charge-coupled device cooled by a thermoelectric device. An excitation light, an argon laser (λ=514.5 nm) or diode laser (λ=780 nm), was focused on a ca. 40-μm-diam spot by a microscope equipped with a long-working-distance objective lens, Mitsutoyo M Plan Apo 10×. Raman spectra were measured using two laser polarizations, i.e., $(b,a+b)$ on the main (001) face and $(c,a+b+c)$ on the edge of the thin-plate-like crystal. Note that the light polarization was almost perpendicular and parallel to the central C═C of ET for $(b,a+b)$ and $(c,a+b+c)$, respectively. Furthermore, both of the polarization directions minimized the high background probably from I_3^-, since the directions were nearly perpendicular to the axis of I_3^-. The $(b,a+b)$ and $(c,a+b+c)$ polarizations were measured with 75 and 25 μW laser powers, respectively (under pressure, these powers were raised by about 50%). A lower laser power was adopted for $(c,a+b+c)$, since the Raman intensity for $(c,a+b+c)$ was higher than that for $(b,a+b)$. The acquisition time of the single spectrum was approximately 60 min.

For the high-pressure Raman experiment, we used a clamped-type diamond-anvil cell, KYOWA CR-DAC-KY04-3, made of BeCu25. To avoid the influence of the strong diamond Raman line at 1332 cm^{-1}, sapphire (0.8-mm-diam culet) was used as an anvil. An Inconel gasket (0.3 mm thick) with a drilled cylindrical hole 0.5 mm in diameter was used as a sample chamber. Single crystals of α-$(ET)_2I_3$ were placed close to the culet of the sapphire and were immersed in the pressure media at a 1:1 mixture of Fluorinart 75 and 77. The pressure regime at low temperature was quasihydrostatic. The laser light penetrated through the sapphire was directly irradiated onto the crystal face in order to diminish the contribution of the pressure media to the collected Raman spectra. As a pressure indicator, we used a ruby fluorescence line, assuming the dependence on a pressure of ca. 0.364 nm/GPa for all temperatures.[37] At room temperature, we applied several pressures up to 3.6 GPa and measured the temperature dependence of the Raman spectra for each subsequently applied pressure. As the temperature was lowered to 20 K, the pressure in the sample chamber

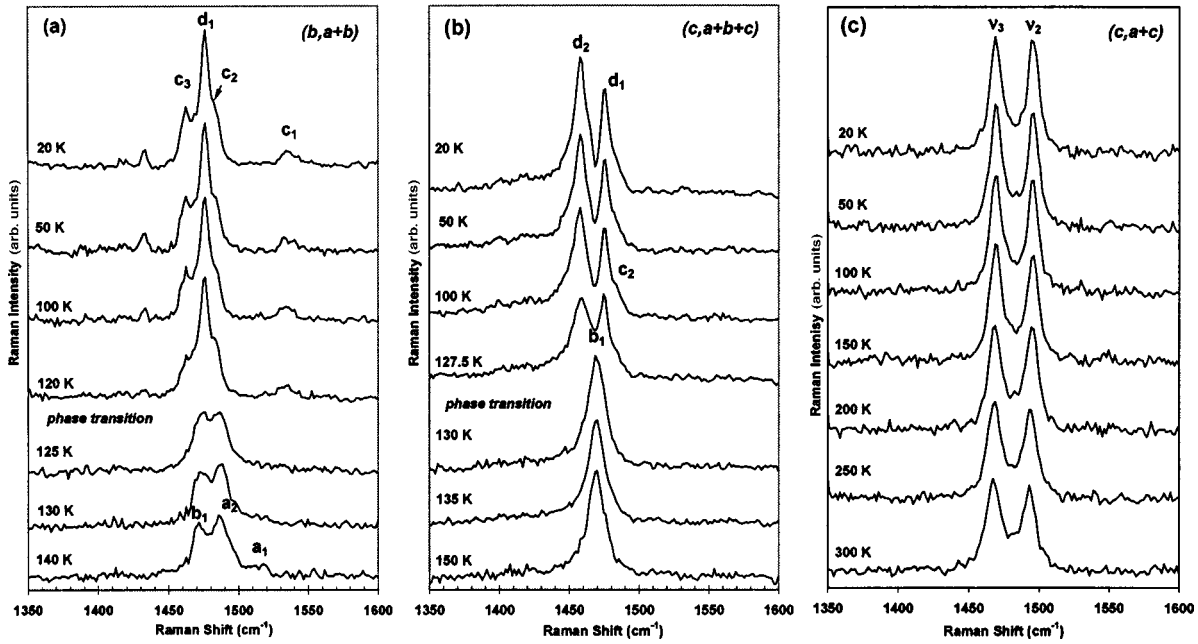

FIG. 2. Temperature dependence of the Raman spectra excited with 514 nm of (a) $(b,a+b)$ and (b) $(c,c+a+b)$ polarizations for α-$(ET)_2I_3$ and (c) the $(c,a+c)$ polarization for θ-$(ET)_2I_3$.

decreased in a pressure range of $0<P<1.5$ GPa, whereas it increased by ca. 0.2 GPa above 1.5 GPa.

III. RESULTS

Figure 2 depicts the temperature dependence of the Raman spectrum of α-$(ET)_2I_3$ and θ-$(ET)_2I_3$ measured at ambient pressure. The molecular arrangement in the conducting layer of θ-$(ET)_2I_3$ is similar to that of α-$(ET)_2I_3$.[38] θ-$(ET)_2I_3$ is metallic down to ca. 4 K, and some crystals show superconductivity at around 3.6 K.[39] As shown in Fig. 2(c), the Raman spectra of metallic θ-$(ET)_2I_3$ exhibits no change on lowering temperature, and well-separated ν_2 and ν_3 modes are clearly observed. On the other hand, abrupt changes were observed at temperatures between 120 and 130 K in the spectra of α-$(ET)_2I_3$ [Figs. 2(a) and 2(b)]. This finding corresponds to the MI phase transition reported in the dc conductivity at $T_{MI}=135$ K. The difference in T_{MI} between the Raman and resistivity measurements is likely to stem from the laser-induced sample overheating in the Raman experiment. The overheating effect for the high-pressure data should be smaller than that obtained at ambient pressure, because the crystal is immersed in a cold pressure medium and the thermal conductivity to a heat sink is much higher than that in a vacuum. Figure 3 shows the comparison of the Raman spectra of α-$(ET)_2I_3$ and α-$(^{13}C(2)\text{-}ET)_2I_3$ at 20 and 150 K. We examined the features of the spectra using two different light sources ($\lambda=514$ and 780 nm) in order to acquire as many peaks as possible. Particularly in the case of the NI phase, the collected data showed noticeable excitation-light dependence [Figs. 3(c) and 3(d)]. We assigned the spectra, as summarized in Table I, by taking account of the polarization, isotope shift, factor group splitting, and pressure dependence. The factor group and pressure dependence will be discussed below. Here we discuss the polarization dependence and isotope shift. The ν_2 and ν_3 modes of $ET^{0.5+}$ involve mainly in-phase ring C═C stretching and central C═C stretching, respectively.[40,41] Therefore, the isotope shift of ν_3 would be expected to be much larger than that of ν_2 (Ref. 40), and the ν_3 mode appears very strongly in the polarization parallel to the long molecular axis of ET (Ref. 42). The spectra of the PM phase [Fig. 3(a)] are characterized by a strong peak $\mathbf{b}_1$ in the $(c,a+b+c)$ polarization and by $\mathbf{a}_1$ and $\mathbf{a}_2$ peaks in the $(b,a+b)$ polarization. The isotope-labeled sample showed another peak $\mathbf{a}_2'$ in addition to $\mathbf{a}_1'$ and $\mathbf{a}_3'$ [Fig. 3(b)]. It is certain that the strong bands of $\mathbf{b}_1$ and $\mathbf{b}_1'$ are attributable to the same mode. The large isotope shift between the $\mathbf{b}_1$ and $\mathbf{b}_1'$ bands $[\omega(\mathbf{b}_1')-\omega(\mathbf{b}_1)=53\ \mathrm{cm}^{-1}]$ indicates that they can be assigned to the ν_3 mode. Two- and three-component bands $\mathbf{a}_1$, $\mathbf{a}_2$ and $\mathbf{a}_1'$, $\mathbf{a}_2'$, $\mathbf{a}_3'$ in the $(b,a+b)$ polarization showed smaller isotope shifts than that of ν_3. Thus they can be attributed to the ν_2 mode. Below T_{MI}, the spectral pattern became more complicated, as shown in Figs. 3(c) and 3(d). As regards α-$(^{13}C(2)\text{-}ET)_2I_3$, the ν_3 bands are clearly separated from those related to ν_2 as a result of the larger isotope downshift of ν_3. In this manner, the $\mathbf{d}_1'$ and $\mathbf{d}_2'$ bands, together with a broad vibronic band $\mathbf{d}_3'$, which was observed only at 780 nm excitation, assigned to ν_3. For the non-isotope-substituted sample, the $\mathbf{d}_1$, $\mathbf{d}_2$, and $\mathbf{d}_3$ bands are attributed to ν_3, since the isotope shifts calculated with respect to $\mathbf{d}_1'$, $\mathbf{d}_2'$, and $\mathbf{d}_3'$ were around 50 cm^{-1}. The more convincing argument in favor of the above assignment is that the $\mathbf{d}_1$ and $\mathbf{d}_2$ bands exhibited high intensity in the $(c,a+b+c)$ polarization and $\mathbf{d}_3$ revealed a broad vibronic feature. The $\mathbf{c}_1'$, $\mathbf{c}_2'$, and $\mathbf{c}_3'$ bands exhibited smaller isotope shifts and higher intensity in the case of $(b,a+b)$, and therefore they

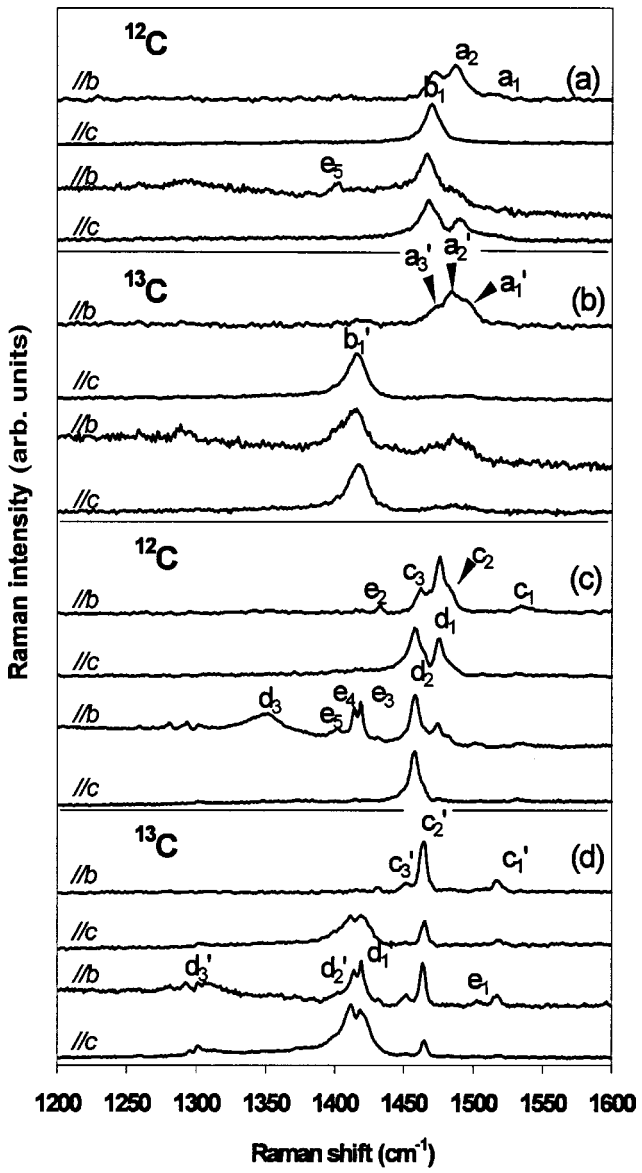

FIG. 3. Raman spectra of α-$(ET)_2I_3$ [(a) and (c)] and α-$(^{13}C(2)\text{-}ET)_2I_3$ [(b) and (d)]. (a) and (b) were taken at 150 K and (c) and (d) at 20 K. In each panel, two top spectra were excited with 514 nm, while two bottom ones with 780 nm. The $\|b$ and $\|c$ indicate the spectra taken in the polarizations of $(b,a+b)$ and $(c,a+b+c)$, respectively.

are attributed to ν_2, as were the corresponding bands at $\mathbf{c}_1$, $\mathbf{c}_2$, and $\mathbf{c}_3$ found in α-$(ET)_2I_3$. If we apply the product rule of Teller-Redlich to the a_g modes of ET, the product ratio $(\nu_2'\nu_3')/(\nu_2\nu_3)$ is expected to be equal to $(m_{C12}/m_{C13})^{1/2}$, where ν_j' and ν_j are, respectively, the frequency of the ν_j mode of $^{13}C(2)$-ET and ET and m_{C12} and m_{C13} are the masses of ^{12}C and ^{13}C, respectively, since the only ν_2 and ν_3 modes show a large isotope shift among the 12 a_g modes of $^{13}C(2)$-ET.[41] As shown in Table I, the product ratio close to the expected value 0.961 supports the assignment for the ν_2 and ν_3 bands. Summarizing the above assignments, in the weakly split ν_2 mode, $\mathbf{a}_1$ and $\mathbf{a}_2$ of α-$(ET)_2I_3$ split more extensively into $\mathbf{c}_1$, $\mathbf{c}_2$, and $\mathbf{c}_3$ below T_{MI} and $\mathbf{a}_1'$, $\mathbf{a}_2'$, and $\mathbf{a}_3'$ of α-$(^{13}C(2)\text{-}ET)_2I_3$ split into $\mathbf{c}_1'$, $\mathbf{c}_2'$, and $\mathbf{c}_3'$. In the same manner, the $\mathbf{b}_1$ band associated with the ν_3 mode splits into $\mathbf{d}_1$, $\mathbf{d}_2$, and $\mathbf{d}_3$ in ^{12}C-ET and $\mathbf{b}_1'$ splits into $\mathbf{d}_1'$, $\mathbf{d}_2'$, and $\mathbf{d}_3'$. Since the frequencies of the ν_2 and ν_3 modes are charge sensitive, the large amount of splitting observed below T_{MI} clearly demonstrated that charge localization, and thus charge disproportionation, occurs below T_{MI}. This observation strongly supports the proposal based on infrared[18] and NMR[22,23] experiments and theoretical prediction.[19,20,21]

The other five bands $\mathbf{e}_1-\mathbf{e}_5$ showed no isotope shift, which indicates that these bands are independent of the central C=C stretching vibration. Among the $\mathbf{e}_1-\mathbf{e}_5$ bands, $\mathbf{e}_2-\mathbf{e}_4$ appeared only below T_{MI} in the $(b,a+b)$ spectra excited with 780 nm in the case of both α-$(ET)_2I_3$ and α-$(^{13}C(2)\text{-}ET)_2I_3$. The $\mathbf{e}_5$ band was also observed in the spectra taken above T_{MI} [see Fig. 3(a)]. The $\mathbf{e}_2-\mathbf{e}_5$ bands are probably due to the CH_2-bending modes such as ν_4 (a_g) and ν_{56} (b_{3g}) or even ν_{28} (b_{1u}) and ν_{45} (b_{2u}).[25,26,27,41] The $\mathbf{e}_1$ band, observed in both α-$(ET)_2I_3$ and α-$(^{13}C(2)\text{-}ET)_2I_3$, can be assigned to the ν_{27} mode, since no other mode except ν_{27} is expected at this frequency.

Figure 4 shows the temperature dependence of the Raman spectra of α-$(ET)_2I_3$ and α-$(^{13}C(2)\text{-}ET)_2I_3$ at approximately fixed pressures. The spectral patterns observed at above 75 K were similar to those measured at ambient pressure for the PM phase [see Figs. 3(a) and 3(b)], with the exception of a small high-frequency shift. The resultant data shows that T_{MI} is located between 75 and 70 K. The lowering of T_{MI} by the application of pressure is consistent with the pressure dependence of the electrical resistivity.[29,30] When the temperature approached T_{MI} from the high-temperature side, the peaks $\mathbf{a}_1$ and $\mathbf{a}_2$ (ν_2 in PM) weakened and three bands at $\mathbf{c}_{1a}$, $\mathbf{c}_{1b}$, and $\mathbf{c}_2$ (ν_2 in NI) increased in intensity. The $\mathbf{c}_3$ band was not seen, since it had overlap with a strong $\mathbf{d}_1$. At the same time, the bands associated with ν_3 ($\mathbf{b}_1$, $\mathbf{b}_2$, $\mathbf{d}_1$, and $\mathbf{d}_2$) also behaved in the same manner as did the ν_2-related bands at around T_{MI}. The $\mathbf{b}_1$ band gradually lost intensity; subsequently, $\mathbf{d}_1$ and $\mathbf{d}_2$ bands appeared. The $\mathbf{d}_2$ band can be observed only in the $(c,a+b+c)$ spectra [Fig. 4(b)]. The doublet nature of the $\mathbf{c}_{1a}$ and $\mathbf{c}_{1b}$ bands was more pronounced in the 780-nm-excitation spectra and was not clearly found in the ambient-pressure spectrum [see Fig. 3(c)]. This trend is consistent with the observation that the $\mathbf{c}_{1a}$ and $\mathbf{c}_{1b}$ bands are more enhanced at higher pressures. On the other hand, $\mathbf{c}_3$ was not observed under pressure, probably due to the overlap with $\mathbf{d}_1$. For α-$(^{13}C(2)\text{-}ET)_2I_3$, as shown in Figs. 4(c) and 4(d), the three components $\mathbf{a}_1'$, $\mathbf{a}_2'$, and $\mathbf{a}_3'$ (ν_2 in PM) changed into four well-separated bands $\mathbf{c}_{1a}'$, $\mathbf{c}_{1b}'$, $\mathbf{c}_2'$, and $\mathbf{c}_3'$ at around T_{MI}. In this compound, the downshifted ν_3 bands did not interfere with the ν_2 bands, but the overlapping with $\mathbf{e}_2-\mathbf{e}_5$ rendered it difficult to rigorously count the number of ν_3 bands.

We measured the pressure-dependent peak shifts in the Raman spectrum of α-$(ET)_2I_3$ at 20, 100, and 150 K to observe the rearrangement of the charge distribution. Figure 5 shows the pressure dependence of the Raman spectrum of α-$(ET)_2I_3$ at 20 K. The observed pressure dependences of the frequencies of ν_2 and ν_3 are plotted in Fig. 6. One can

TABLE I. Assignment of ν_2 and ν_3 modes for θ-$(ET)_2I_3$, α-$(ET)_2I_3$, and α-$(^{13}C\text{-}ET)_2I_3$. $\Delta\omega$ is the isotope shift observed in the α phase. s: shoulder. b: broad peak. vb: very broad peak with a dip. $\langle a_j \rangle$ denotes the average value of the frequency of a_j ($j=1,2$, and 3) assuming that a_2 and a_3 is degenerate in unsubstituted compound.

Temperature (K)	a_g modes	θ-$(ET)_2I_3$ (cm^{-1})	α-$(ET)_2I_3$ (cm^{-1})	α-$(^{13}C\text{-}ET)_2I_3$ (cm^{-1})	$\Delta\omega$ (cm^{-1})
150	ν_2	$a=1495$	$a_1=1511$(s) $a_2, a_3=1487$	$a_1'=1495$(s) $a_2'=1483$ $a_3'=1475$(s)	$\Delta\overline{\omega}=11$
	ν_3	$b=1469$	$b_1=1470$	$b_1'=1417$	53
	$\frac{\langle a_j' \rangle b_1'}{\langle a_j \rangle b_1}$		0.957		
20	ν_2	$a=1495$	$c_1=1533$ $c_2=1481$(s) $c_3=1462$	$c_1'=1517$ $c_2'=1465$ $c_3'=1452$	16 16 10
	ν_3	$b=1469$	$d_1=1476$ $d_2=1458$ $d_3=1352$(b)	$d_1'=1423$ $d_2'=1410$ $d_3'=1303$(vb)	53 48 49
	$\frac{c_j' d_j'}{c_j d_j}$		0.954 ($j=1$) 0.957 ($j=2$) 0.957 ($j=3$)		

see that the spectrum shows remarkable peak shifts, depending upon the pressure both in the PM ($P>1.5$ GPa) and NI ($P<1.2$ GPa) phases. In the PM phase above 1.5 GPa, all Raman bands showed an upshift with increasing pressure. It should be noted that the application of pressure generally hardens vibrational modes. To examine this effect from the obtained data, we measured the pressure dependence of the Raman spectra of a stable metallic compound θ-$(ET)_2I_3$. The results measured at 20, 100, and 150 K are also shown in Fig. 6. The gradient of the nearly linear relationship between frequency and pressure was obtained as $d\omega/dP \approx 4-5\ cm^{-1}\ GPa^{-1}$ (see Fig. 6). This value is considered as the pressure effect simply resulting from the lattice contraction.[43] Analogous behavior was observed in the spectra of the PM phase at 100 K ($P>0.4$ GPa) and 150 K ($P>0$ GPa), as shown in Figs. 6(a) and 6(b). Nevertheless, $d\omega/dP$ of $\mathbf{a}_2$ was slightly higher than that of $\mathbf{a}_1$, e.g., $\Delta(d\omega/dP) \approx 2-3\ cm^{-1}\ GPa^{-1}$. This finding indicated that the splitting of ν_2 tends to be slightly suppressed under pressure in the PM phase. However, the suppression degree is much smaller than that found in the NI phase. The pressure dependence of the spectrum of the NI phase is very different from that of the PM phase. In the NI phase below 1.2 GPa, the $\mathbf{c}_{1a}$ and $\mathbf{c}_{1b}$ bands revealed a very pronounced downshift. The gradient $d\omega/dP$ is estimated as ca. $-9\ cm^{-1}\ GPa^{-1}$. On the other hand, the $\mathbf{c}_2$ and $\mathbf{c}_3$ bands revealed an upshift. The $\mathbf{c}_3$ band shifted up over 10 cm^{-1} and eventually overlapped with $\mathbf{d}_1$ above 0.55 GPa. Therefore, the $d\omega/dP$ of $\mathbf{c}_3$ is probably as high as 20 $cm^{-1}\ GPa^{-1}$. These peculiar pressure dependences cannot be understood as a result of the lattice contraction, but instead are ascribed to the continuous modification of the charge distribution by pressure, since the frequencies of ν_2 and ν_3 are sensitive to the molecular charge. The observed behavior indicates that the ν_2 bands of the charge-rich sites ($\mathbf{c}_2, \mathbf{c}_3$) and charge-poor sites ($\mathbf{c}_{1a}, \mathbf{c}_{1b}$) approach each other with increasing pressure. Therefore, the charge disproportionation tends to be suppressed by pressure. The $\mathbf{d}_1$ band also showed an upshift upon pressure. Since ν_3 is more or less EMV coupled,[44] the upshift was the result not only of the change in the charge distribution, but also of the change in transfer integrals.

IV. DISCUSSION

Before discussing the charge distribution in the unit cell more quantitatively, let us briefly view the factor group analysis. Table II shows the correlation diagram of a_g mode in α-$(ET)_2I_3$. As the space group is $P\overline{1}$ above T_{MI}, four a_g modes (four molecules in the unit cell) are classified into $\Gamma(4a_g)=3A_g+A_u$ and theoretically three A_g modes can appear as Raman-active bands. If the three Raman-active modes derived from the charge-sensitive ν_2 mode are observed, the splitting may reflect the nonuniform charge density at the three crystallographically nonequivalent sites. If we take a tight-binding band model, the difference in charge density at the crystallographically nonequivalent sites is ascribed to the set of transfer integrals and site-energy differences. Since the unit cell of α-$(ET)_2I_3$ contains four ET molecules, the highest occupied molecular orbital (HOMO) band consists of four split bands.[7] The seven transfer integrals given by Mori *et al.* provide a semimetal band, in which holes partially occupy the fourth and third bands.[7] The

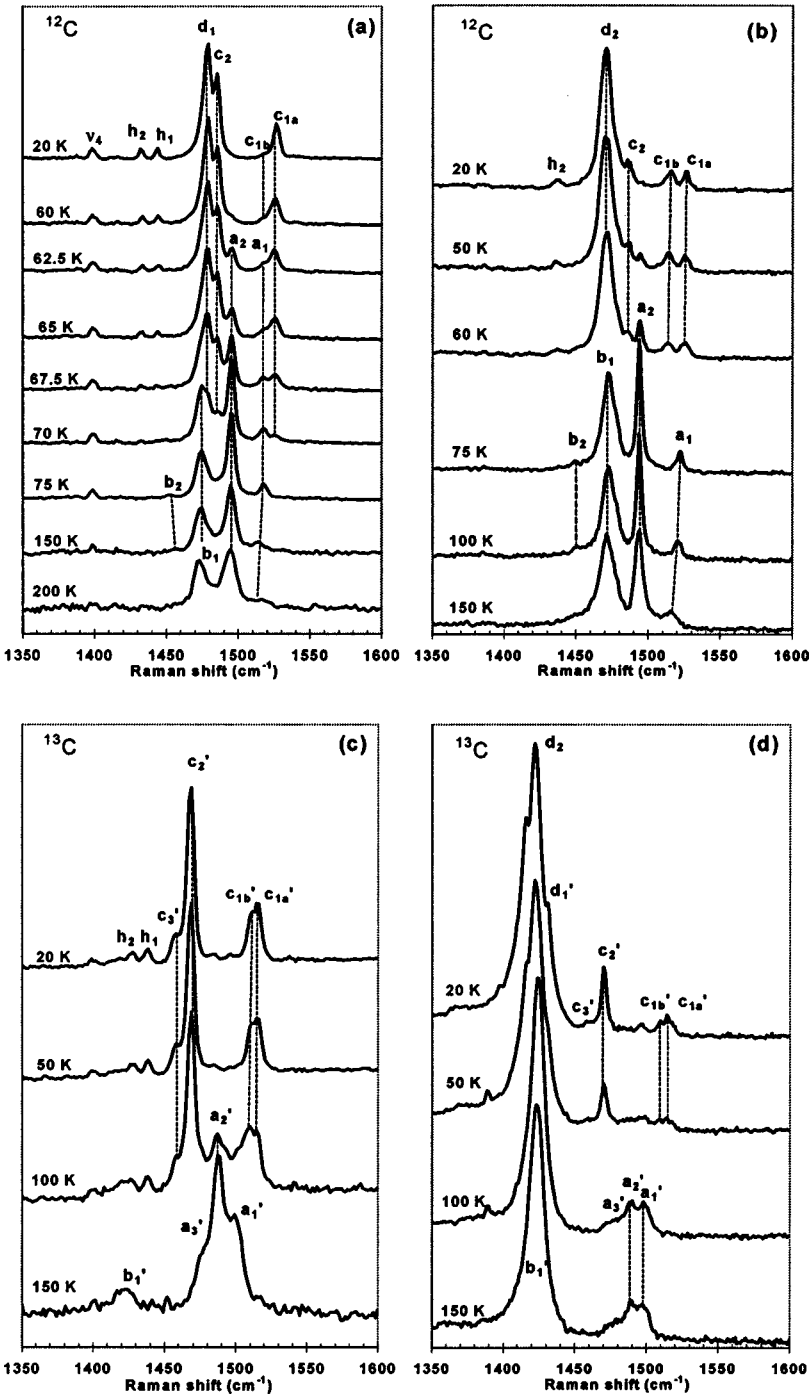

FIG. 4. Temperature dependence of the Raman spectra of α-$(ET)_2I_3$ [(a) and (b)] measured at 0.60 GPa and α-(^{13}C(2)-$ET)_2I_3$ [(c) and (d)] at 0.45 GPa. (a) and (c) were measured with 514 nm and $(b,a+b)$ polarization and (b) and (d) with 780 nm and $(c,a+b+c)$ polarization.

site-energy difference comes from the Coulomb interactions with the counter anion I_3^-. The charge density at the jth site can be calculated by the following equation:

$$\rho_j = \sum_{ka,kb} \sum_{m=1}^{4} \langle km|n_j|km\rangle f(\varepsilon), \tag{1}$$

where $|km\rangle$ is the Bloch function of the mth band, n_j is the number operator at the jth site, and $f(\varepsilon)$ is the Fermi-Dirac function for a hole. Using ρ_j, the charge distribution in the unit cell is expressed in such manner as $A^{\rho_A{}^+} A'^{\rho_{A'}{}^+} B^{\rho_B{}^+} C^{\rho_C{}^+}$ [see Fig. 1(a)]. Assuming that the site energy is the same at every site, we numerically calculated the eigen function $|km\rangle$ of the tight-binding band and found that the site charge given by Eq. (1) was approximately expressed like $\rho_A = \rho_{A'} = \rho_B = 0.5 + \delta_M$ and $\rho_C = 0.5 - 3\,\delta_M$: i.e., site **C** is charge poor and the other three sites **A**, **A′**, and **B** are slightly charge rich. This inhomogeneity is reduced by the introduction of on-site Coulomb energy U. According to Kino and Fukuyama by the mean-field calculation for a smaller U (i.e., in the semimetal region), δ_M is calculated to be about 0.03.[20]

Interestingly, the ν_2 mode in the PM phase of α-$(ET)_2I_3$ was split into two bands $\mathbf{a}_1$ and $\mathbf{a}_2$, as shown in Fig. 3(a),

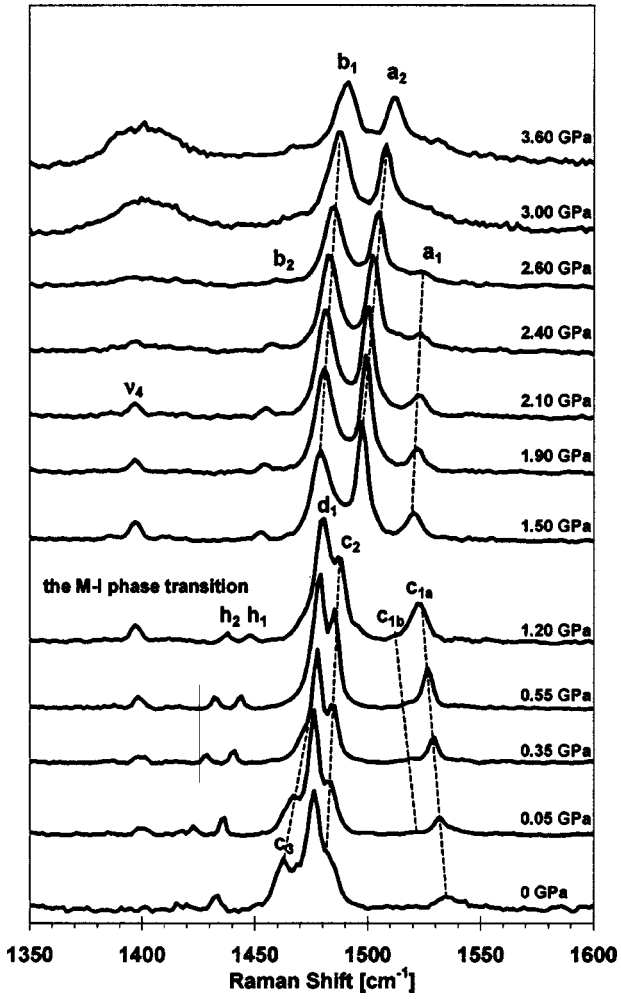

FIG. 5. Pressure dependence of the Raman spectra of α-$(ET)_2I_3$ at 20 K excited with 514 nm for the $(b,a+b)$ polarization.

Fig. 4(a) ($T>75$ K), Fig. 4(b) ($T>75$ K), and Fig. 5 ($P>1.5$ GPa). The $\mathbf{a}_1$ and $\mathbf{a}_2$ bands are, respectively, assigned to the ν_2 mode at the charge-rich and charge-poor sites. To roughly estimate δ_M from the experimental data, we used the linear relation between the charge on ET and the frequency of ν_2, since ν_2 is coupled much more weakly than is ν_3 with an electronically excited state via EMV interaction.[24] To be more precise, the frequency of ν_2 against the molecular charge is not linear, because the degree of mixing with ν_3 depends upon the molecular charge. However, the linear relation is a sufficient approximation for a rough estimation, which is described in the Appendix. Within the linear approximation, δ_M is estimated from the equation

$$\delta_M = \frac{1}{4}\,\frac{\nu_2(\mathbf{a}_2)-\nu_2(\mathbf{a}_1)}{\nu_2(0)-\nu_2(1+)}, \tag{2}$$

where $\nu_2(0)=1552\ \mathrm{cm}^{-1}$ and $\nu_2(1+)=1462\ \mathrm{cm}^{-1}$.[24,26] Figure 7 shows the pressure dependence of δ_M at 20, 100, and 150 K. As shown in this figure, $\delta_M \sim 0.05$ is almost pressure independent. Therefore, the hole density at the **A**, **A**′, and **B** sites in the PM phase is estimated at about 0.55+ and the corresponding value at the **C** site is about 0.35+.

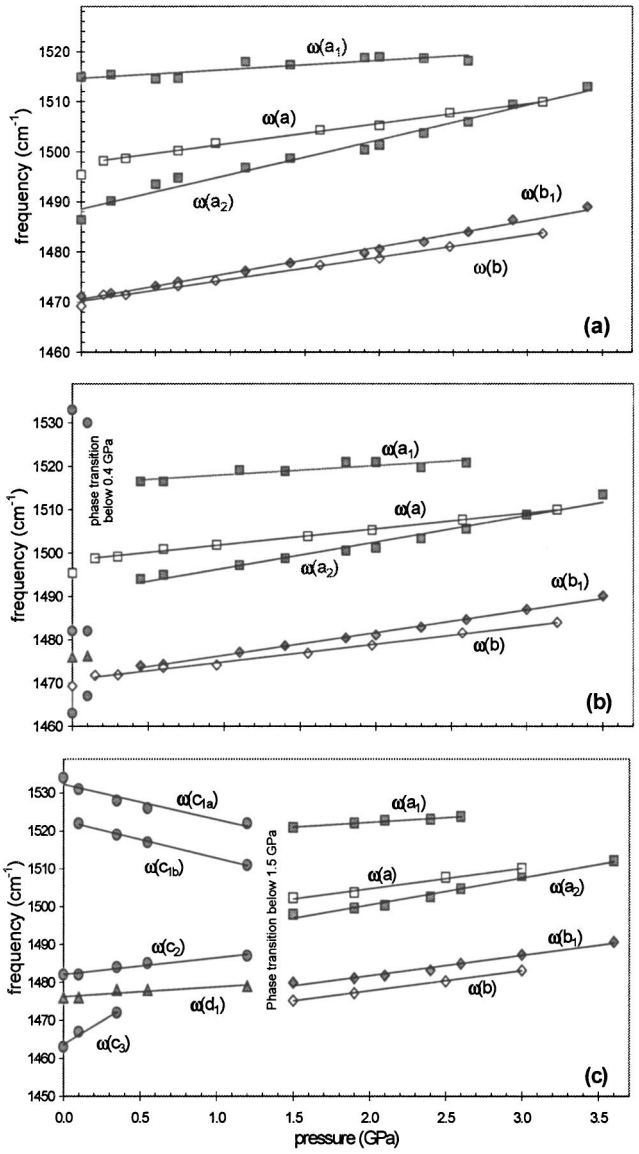

FIG. 6. Pressure dependence of the band frequencies observed at (a) 150 K, (b) 100 K, and (c) 20 K in α-$(ET)_2I_3$ and θ-$(ET)_2I_3$. The spectra of the former and latter compounds were taken with 514 nm excitation and $(b,a+b)$ and $(a,a+c)$ polarizations, respectively. The gray symbols represent the bands observed in the α phase, while the open symbols denote the bands recorded in the θ phase.

The agreement with the theoretical calculation is very good. For α-(^{13}C(2)-ET)$_2I_3$, the ν_2 mode in the PM phase consists of three bands $\mathbf{a}_1'$, $\mathbf{a}_2'$, and $\mathbf{a}_3'$ [see Figs. 3(c), 4(c), and 4(d)]. The further splitting of the ν_2 mode of α-(^{13}C(2)-ET)$_2I_3$ can be explained by the charge-dependent isotope shift, which is discussed in the Appendix. The $\mathbf{a}_1$ band slowly weakened upon pressure, and still weakly remained, even at 3.6 GPa (see Fig. 5), which indicates that the charge distribution is nonuniform up to 3.6 GPa. The separation between the $\mathbf{a}_1$ and $\mathbf{a}_2$ bands was almost pressure independent, and thus δ_M was also nearly independent of pressure up to 3.6 GPa. The high-pressure x-ray diffraction experiment indicates that the unit cell of α-$(ET)_2I_3$ shows

TABLE II. Correlation diagram of a_g modes (ν_2 and ν_3) among the molecule, site, and unit-cell symmetry.

	Molecule symmetry	Space group	Site symmetry	Factor group	$\Gamma(4a_g)$
	D_{2h}	$P\bar{1}$ ($T>T_{\mathrm{MI}}$)	$C_i(B,C)$ $C_1(A,A')$	C_i	
		$P1$ ($T<T_{\mathrm{MI}}$)	C_1	C_1	
ν_2, ν_3	$4a_g$	$P\bar{1}$ ($T>T_{\mathrm{MI}}$)	$2a_g(B,C)$ $2a(A,A')$	$2a_g(B,C)$ $\begin{cases}1a_g(A,A')\\1a_u(A,A')\end{cases}$	$3A_g+A_u$
		$P1$ ($T<T_{\mathrm{MI}}$)	$4a$	$4a$	$4A$

almost isotropic contraction upon pressure, and the dihedral angle between ET molecules in different stacks does not change within the limits of experimental error.[45] If the lattice contraction is isotropic, every transfer integral would be expected to increase in the same manner. In such a situation, the charge distribution calculated by Eq. (1) hardly changes. Therefore, the splitting of the ν_2 mode, and thus the inhomogeneous charge distribution in the PM phase, can be explained very well by the band picture. Tajima *et al.* reported the transport properties of α-$(ET)_2I_3$ under 2.0 GPa. They proposed a very narrow-gap semiconductor model with the hole mobility as high as 3×10^5 $cm^2/V\,s$ at about 1.5 K. This model implies that the charge carriers are moving coherently in harmony with the band picture. Our results in the PM phase at 20, 100, and 150 K are consistent with their model.

Let us now turn our attention to the spectrum of the NI phase. If the inversion symmetry is broken at T_{MI}, the symmetry representations for the NI phase changes into $\Gamma(4a_g)=4A$ (see Table II). In such a case, we may expect the appearance of four peaks attributable to ν_2. At ambient pressure, only three ν_2-related bands (see Table I) were observed in the Raman spectra at temperatures below T_{MI}, probably because of their low intensity. However, under high pressure, the four bands associated with ν_2 were identified both in α-$(ET)_2I_3$ [see $\mathbf{c}_1$, $\mathbf{c}_2$, and $\mathbf{c}_3$ in Fig. 3(c) and $\mathbf{c}_{1a}$, $\mathbf{c}_{1b}$, and $\mathbf{c}_2$ in Figs. 4(a) and 4(b)] and in α-$(^{13}C(2)\text{-}ET)_2I_3$ [see $\mathbf{c}'_{1a}$, $\mathbf{c}'_{1b}$, $\mathbf{c}'_2$, and $\mathbf{c}'_3$ in Figs. 4(c) and 4(d)]. The presence of four ν_2 bands indicates the breaking of the inversion symmetry in the NI phase. This symmetry change might be related to the splitting of the stretching modes of I_3^- below 103 K in α-$(ET)_2I_3$.[46] The disappearance of inversion symmetry indicates that the **A** and **A′** sites are no longer equivalent to each other, $\mathbf{A}\neq\mathbf{A}'$. As shown in Fig. 5 ($P<1.2$ GPa), the four bands are grouped into two pairs, i.e., $\mathbf{c}_{1a}$, $\mathbf{c}_{1b}$ and $\mathbf{c}_2$, $\mathbf{c}_3$, which correspond to the ν_2 mode at the charge-poor and charge-rich sites, respectively. There are six possible ways to assign the two charge-rich sites among the four sites in the unit cell. The paramagnetic susceptibility of α-$(ET)_2I_3$ exhibits an abrupt drop at 135 K and decreases toward zero with an activation energy of $\sim$500 K.[15] Seo analyzed the susceptibility in the NI phase using the alternating Heisenberg model employing the relation of $J\sim4t^2/U$, where J and t are, respectively, the exchange energy and transfer integral between the holes and U is the on-site Coulomb energy. Based on this analysis, he proposed a horizontal stripe along the zigzag line *ABAB*... as the array of the localized positive charge.[21] This conclusion is based on the large transfer integrals between **A**(0,0) and **B**(0,0), between **A**(0,0) and **C**(0,0), between **C**(0,0) and **A′**(0,1), and between **A′**(0,1) and **B**(−1,0), where the numbers in parentheses denote the translation along the *a* and *b* axes. These pairs can form a spin singlet. This model requires the breaking of inversion symmetry, which was confirmed in this experiment. If we follow this model, the charge-rich site is (**A**,**B**), (**A**,**C**), (**C**,**A′**), or (**A′**,**B**). Other evidence supporting the horizontal stripe model is the observation of a new weak electronic absorption band at about 7500 cm^{-1} in the $E\|b$ spectrum below T_{MI} (see Fig. 9 of Ref. 47). This electronic transition is associated with the excited state involving U, which corresponds to the charge-transfer excitation between

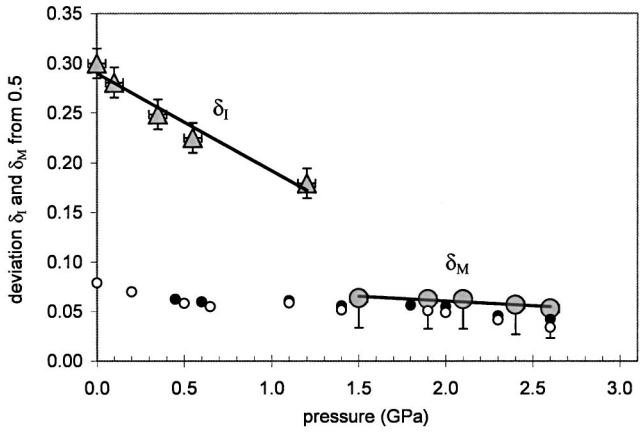

FIG. 7. Pressure dependence of δ_I (gray triangle) and δ_M (gray circle) at 20 K calculated from ν_2 bands shown in Fig. 5. The data δ_M calculated from the spectra measured at 100 and 150 K are drawn by ● and ○, respectively. See the text for the definition of δ_I and δ_M.

the charge-rich sites. The polarization direction of this transition is expected to be parallel to the direction connecting the centers of the charge-rich sites; for example, the direction connecting the **A** and **B** sites forms angles of 67° and 22° with respect to the *a* and *b* axes, respectively. We also measured the $E\|a$ and $E\|b$ spectra in the 600–10 000 cm^{-1} range above (150 K) and below (50 K) T_{MI}, and confirmed that this new band was observed only in the $E\|b$ spectrum at 50 K (not shown). As discussed later, the charge-rich site **C** in the PM phase seems to be preserved in the NI phase. If we assume that the charge-poor site in the PM phase remains charge poor in the NI phase, (**A**,**B**) or (**A**′,**B**) will be the charge-rich site. Therefore, in the former case, for example, the charge distribution in the unit cell can be described as $\mathbf{A}^{(0.5+\delta_A)+}\mathbf{A}'^{(0.5-\delta_{A'})+}\mathbf{B}^{(0.5+\delta_B)+}\mathbf{C}^{(0.5-\delta_C)+}$ with a conditional equation $\delta_A+\delta_B=\delta_{A'}+\delta_C$. We estimate the average value $\delta_I=(\delta_A+\delta_B)/2$ from the frequency difference between the midpoint of $\mathbf{c}_{1a}$ and $\mathbf{c}_{1b}$ and the midpoint of $\mathbf{c}_2$ and $\mathbf{c}_3$ using a relation similar to Eq. (2). Since the $\mathbf{c}_3$ band merges with the $\mathbf{d}_1$ band above 0.55 GPa, the frequency of $\mathbf{c}_3$ at 0.55 and 1.2 GPa was estimated from the extrapolation of the data obtained at 0, 0.05, and 0.35 GPa. Since we use the frequency difference, the pressure effect shown in Fig. 7 for θ-$(ET)_2I_3$ is canceled out in this analysis. At first glance at Fig. 5, one can see that the ν_2 bands at the charge-rich and charge-poor sites are approaching each other with increasing pressure. Correspondingly, δ_I, drawn in Fig. 7, decreases with increasing pressure. At ambient pressure, δ_I is calculated to be ca. 0.3. With increasing pressure, δ_I is almost linearly reduced to less than 0.2 at 1.2 GPa. Therefore, δ_I changes by ca. 0.1/GPa in the NI phase. In this manner, pressure acts as an external parameter that tunes the charge-disproportionation ratio in the NI state. This is the manifestation of the direct competition between t and V, where the pressure leads to a faster increase in t than V. The α phase of $(ET)_2I_3$ is a good example of such competition, since the unit cell almost isotropically shrinks without changing the dihedral angles between ET molecules under pressure; in other words, the intermolecular distances are shortened without changing the molecular arrangement.[45] The localized charge is probably ordered in the range of $P<0.6$ GPa and $T\sim 20$ K, where the resistivity value at 20 K is five orders of magnitude higher than the room-temperature value $\rho(20\text{ K})/\rho(300\text{ K})>10^5$. However, at 1.2 GPa, the resistivity is drastically reduced to $\rho(20\text{ K})/\rho(300\text{ K})\sim 10$. In this region ($T\sim 20$ K, $P\sim 1.2$ GPa), the ordered charge becomes more mobile: i.e., the charge gap is reduced to a great extent by the enhanced transfer integrals. The reduction of the charge gap parallel to the charge-disproportionation ratio by the enhanced t/U and t/V is consistent with mean-field theory.[19,20,21] It is of interest to examine the pressure-dependent charge distribution at the PM/NI boundary. As shown in Figs. 5 and 6(c), the $\mathbf{c}_{1a}$ band approaches the $\mathbf{a}_1$ band at the **C** site, while $\mathbf{c}_{1b}$, $\mathbf{c}_2$, and $\mathbf{c}_3$ appear to converge to $\mathbf{a}_2$ at the **A**, **A**′, and **B** sites. These findings suggest that the most charge-poor site is preserved at **C** and the rearrangement of the charge distribution occurs among **A**, **A**′, and **B**. However, as shown in Fig. 6(c), the linear extrapolation of the frequency of these bands shows gaps at around 1.5 GPa. Therefore, the rearrangement of the charge distribution occurs discontinuously at around 1.5 GPa, which is regarded as the melting of the ordered charge.

V. CONCLUSIONS

We measured the Raman spectra of α-$(ET)_2I_3$ below and above the metal-insulator phase transition temperature (T_{MI}) under ambient and quasihydrostatic pressures up to 3.6 GPa. The data confirmed that the nonstructural metal-insulator phase transition of α-$(ET)_2I_3$ is due to the phase transition to the CO state. At temperatures above T_{MI} in the semimetallike phase, the splitting of ν_2 indicated a small deviation from the uniform charge distribution in the unit cell, which was nearly independent of pressure. This inhomogeneous

TABLE III. Frequency of the ν_2 and ν_3 modes, depending on the molecular charge ρ of natural (ET) and isotope-labeled [^{13}C(2)-ET and ^{13}C(6)-ET] molecules.

Mode	Ionicity ρ	ET	^{13}C(2)-ET central C═C[a]	^{13}C(6)-ET central and ring C═C[a]	Reference
ν_2	+0	1552	1523 (29)	1487 (65)	40
	+0.15	1543	1525 (18)		24
	+0.2	1533	1517 (16)		This study
	+0.3	1525	1510 (15)		This study
	+0.5	1503	1500 (3)		42
	+0.5	1497		1436 (61)	40
	+0.7	1485	1472 (13)		This study
	+0.8	1481	1465 (16)		This study
	+0.85	1480	1461 (19)		24
	+1	1462			26
ν_3	+0	1494	1465 (29)	1437 (57)	40
	+0.5	1469	1421 (48)	1415 (54)	40, 42
	+1	1411			26

[a]Values in parentheses are the isotope shifts.

charge distribution was interpreted based on the band model without the localized nature of the charge. The large splitting of ν_2 in the insulating phase indicated that the charge disproportionation was caused by charge localization. Holes occupied two sites (charge-rich sites) with a different charge density, and these charge-rich sites formed a horizontal stripe perpendicular to the stacks. The charge-disproportionation ratio, estimated at ambient pressure to be on average 0.2–0.8, decreased with pressure by ca. $0.1e$/GPa, and eventually the charge disproportionation was discontinuously suppressed at around 1.5 GPa. This pressure dependence of the charge-disproportionation ratio was related to the competition between transfer integrals and intersite Coulomb repulsion.

ACKNOWLEDGMENTS

This research was supported by a Grant-in-Aid for Scientific Research (Nos. 13440214 and 13-01080) from the Ministry of Education, Culture, Sports, Science and Technology of Japan. This study was also supported by the Japan Society for Promotion of Science.

APPENDIX: NONLINEAR IONICITY DEPENDENCE OF ν_2 IN ^{13}C(2)-ET

We did not perform a quantitative analysis of the Raman data of α-(^{13}C(2)-ET)$_2$I$_3$ because the deviation from the linear approximation for the estimation of δ is much larger than that of α-(ET)$_2$I$_3$. Below, we discuss the difference between ET and ^{13}C(2)-ET from the viewpoint of the ionicity dependence of the frequency of the ν_2 mode. When all atoms constituting C═C are isotope substituted [^{13}C(6)-ET], both ν_2 and ν_3 are downshifted according to the Redlich-Teller rule by a maximum of ca. 60 cm^{-1}.[40] Since the central and ring C═C stretching modes are almost equally mixed in the ν_2 and ν_3 modes of (ET)^0, both ν_2 and ν_3 are equally shifted by ca. 30 cm^{-1} in (^{13}C(2)-ET)^0.[40] Table III shows this relationship when the ionicity is $\rho=0$. This table further shows the ionicity dependence of the frequencies of ν_2 and ν_3 of ET and ^{13}C(2)-ET. Eldridge *et al.* demonstrated that the stretching mode of the central and ring C═C is almost decoupled for (ET)$^{0.5+}$ (in 1:2 salts).[40] Actually, the isotope shift of ν_2 is very small,[42] whereas that of ν_3 is ca. 50 cm^{-1} in (^{13}C(2)-ET)$^{0.5+}$. Therefore, the isotope shift of ν_2 is thought to indicate the degree of mixing. As regards the degree of mixing in (ET)$^{1+}$, no isotope shift data are available at the present time. We estimate the isotope shift to be in the region of $0.5<\rho<1$ from the charge-rich site in the CO state of α-(ET)$_2$I$_3$ and θ-(ET)$_2$RbZn(SCN)$_4$. The results are shown in Fig. 8, along with the isotope shift of the $0<\rho<0.5$ region estimated from the charge-poor site. Interestingly, the isotope shift of the $0.5<\rho<1$ region is similar to the mirror image of that of the $0<\rho<0.5$ region. Therefore, we speculate from the extrapolation that the isotope shift of (ET)$^{1+}$ resembles that of (ET)^0. This result implies that the mixing between the central and ring C═C stretching modes decreases toward the decoupled state in the $0<\rho<0.5$ region and increases toward the equally coupled state in the $0.5<\rho<1$ region. This ionicity dependence causes the nonlinear dependence of the ν_2 frequency on the molecular charge of ET. As shown in Table III, the frequency versus charge of ν_2 in ET gives a weakly concave curve. Therefore, the frequency versus charge reveals a strongly convex curve in ^{13}C(2)-ET. This nonlinear ionicity dependence can account for why ν_2 in the PM phase splits into three $\mathbf{a}_1'$, $\mathbf{a}_2'$, and $\mathbf{a}_3'$ bands in α-(^{13}C(2)-ET)$_2$I$_3$. Since the slope in the $0.5<\rho<1$ region is steeper than that of ET, the bands $\mathbf{a}_2'$ and $\mathbf{a}_3'$, which correspond to the charge-rich sites, are well resolved in α-(^{13}C(2)-ET)$_2$I$_3$.

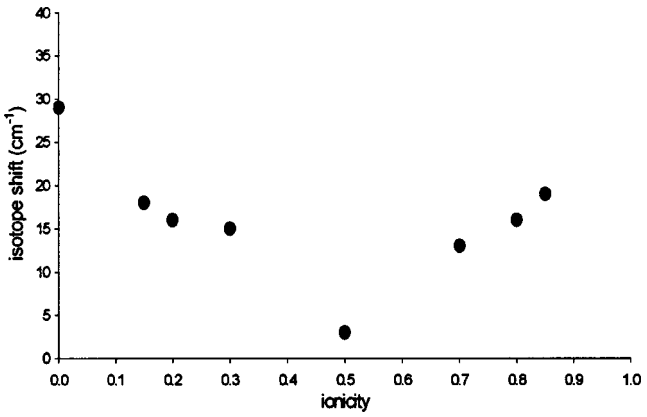

FIG. 8. Isotope shift $\Delta\nu_2=\nu_2$(ET)-ν_2(^{13}C(2)-ET) against the ionicity ρ in ET$^{\rho+}$.

*Permanent address: Department of Molecular Physics, Faculty of Chemistry, Technical University of Lodz, Zeromskiego 116, 90-924, Lodz, Poland.

[1] J. M. Williams, J. R. Ferraro, R. J. Thorn, K. D. Carlson, U. Geiser, H. H. Wang, A. M. Kini, and M. H. Whangbo, *Organic Superconductors (Including Fullerenes): Synthesis, Structure, Properties, and Theory* (Prentice-Hall, Englewood Cliffs, NJ, 1992).

[2] T. Ishiguro, K. Yamaji, and G. Saito, *Organic Superconductors*, Series in Solid State Science (Springer-Verlag, Berlin, 1998).

[3] E. B. Yagubskii, I. F. Shchegolev, V. N. Laukhin, P. A. Kononovich, M. V. Karatsovnik, A. V. Zvarykina, and L. I. Buravov, JETP Lett. **39**, 12 (1984).

[4] H. Kobayashi, R. Kato, A. Kobayashi, Y. Nishio, K. Kajita, and W. Sasaki, Chem. Lett. **1986**, 789 (1986); **1986**, 833 (1986); **1986**, 957 (1986).

[5] A. Kobayashi, R. Kato, H. Kobayashi, S. Moriyama, Y. Nishio, K. Kajita, and W. Sasaki, Chem. Lett. **1987**, 459 (1987); **1987**, 507 (1987).

[6] K. Bender, I. Henning, D. Schweitzer, K. Dietz, H. Endres, and H. J. Keller, Mol. Cryst. Liq. Cryst. **108**, 359 (1984).

[7] T. Mori, A. Kobayashi, Y. Sasaki, H. Kobayashi, G. Saito, and H. Ionokuchi, Chem. Lett. **1984**, 957 (1984).

[8] H. Endres, H. J. Keller, R. Swietlik, D. Schweitzer, K. Angermund, and C. Kruger, Z. Naturforsch. Teil A **41**, 1319 (1986).

[9] T. J. Emge, P. C. W. Leung, M. A. Beno, H. H. Wang, and J. M.

Williams, Mol. Cryst. Liq. Cryst. **138**, 393 (1986).
[10] Y. Nogami, S. Kagoshima, T. Sugano, and G. Saito, Synth. Met. **16**, 367 (1986).
[11] M. Meneghetti, R. Bozio, and C. Pecile, J. Phys. (Paris) **47**, 1377 (1986).
[12] M. Meneghetti, R. Bozio, and C. Pecile, Synth. Met. **19**, 143 (1987).
[13] C. P. Heidmann, A. Barnsteiner, F. Grob-Alltag, B. S. Chandrasekhar, and E. Hess, Solid State Commun. **84**, 711 (1992).
[14] B. Rothaemel, L. Forro, J. R. Cooper, J. S. Schilling, M. Weger, P. Bele, H. Brunner, D. Schweitzer, and H. J. Keller, Phys. Rev. B **34**, 704 (1986).
[15] T. Sugano, G. Saito, and M. Kinoshita, Phys. Rev. B **34**, 117 (1986).
[16] M. Dressel, G. Gruner, J. P. Pouget, A. Breining, and D. Schweitzer, J. Phys. I **4**, 579 (1994).
[17] N. A. Fortune, K. Murata, M. Ishibashi, M. Tokumoto, N. Kinoshita, and H. Anzai, Solid State Commun. **77**, 265 (1991).
[18] J. Moldenhauer, Ch. Horn, K. I. Pokhodnia, D. Schweitzer, I. Heinen, and H. J. Keller, Synth. Met. **60**, 31 (1993).
[19] H. Kino and H. Fukuyama, J. Phys. Soc. Jpn. **64**, 1877 (1995).
[20] H. Kino and H. Fukuyama, J. Phys. Soc. Jpn. **65**, 2158 (1996).
[21] H. Seo, J. Phys. Soc. Jpn. **69**, 805 (2000).
[22] Y. Takano, K. Hiraki, H. M. Yamamoto, T. Nakamura, and T. Takahashi, Synth. Met. **120**, 1081 (2001).
[23] Y. Kubo, Y. Takano, K. Hiraki, T. Taahashi, H. Yamamoto, and T. Nakamura, Synth. Met. **133-134**, 307 (2003).
[24] K. Yamamoto, K. Yakushi, K. Miyagawa, K. Kanoda, and A. Kawamoto, Phys. Rev. B **65**, 085110 (2002).
[25] M. E. Kozlov, K. I. Pokhodnia, and A. A. Yurchenko, Spectrochim. Acta, Part A **43**, 323 (1986).
[26] H. H. Wang, R. Ferraro, J. M. Williams, U. Geiser, and A. Schlueter, J. Chem. Soc., Chem. Commun. **1994**, 1893 (1994).
[27] H. H. Wang, A. M. Kini, and J. M. Williams, Mol. Cryst. Liq. Cryst. Sci. Technol., Sect. A **284**, 211 (1996).
[28] H. Schwenk, F. Gross, C.-P. Heidmann, K. Andres, D. Schweitzer, and H. Keller, Mol. Cryst. Liq. Cryst. **119**, 329 (1985).
[29] M. V. Kartsovnik, P. A. Kononovich, V. N. Laukhin, A. G. Khomenko, and I. F. Shchegolev, Sov. Phys. JETP **61**, 866 (1985).
[30] N. Tajima, M. Tamura, Y. Nishio, K. Kajita, and Y. Iye, J. Phys. Soc. Jpn. **69**, 543 (2000).
[31] S. Mazumdar, R. T. Clay, and D. K. Campbell, Phys. Rev. B **62**, 13 400 (2000).
[32] J. Merio and R. H. McKenzie, Phys. Rev. Lett. **87**, 237002 (2001).
[33] N. Tajima, A. Ebina-Tajima, M. Tamura, Y. Nishio, and K. Kajita, J. Phys. Soc. Jpn. **71**, 1832 (2002).
[34] H. Anzai, M. Tokumoto, T. Ishiguro, G. Saito, H. Kobayashi, R. Kato, and A. Kobayashi, Synth. Met. **19**, 611 (1987).
[35] A. Kawamoto, K. Miyagawa, Y. Nakazawa, and K. Kanoda, Phys. Rev. B **52**, 15 522 (1995).
[36] K. Yakushi, H. Kanbara, H. Tajima, H. Kuroda, G. Saito, and T. Mori, Bull. Chem. Soc. Jpn. **60**, 4251 (1987); M. Tamura, K. Yakushi, H. Kuroda, A. Kobayashi, R. Kato, and H. Kobayashi, J. Phys. Soc. Jpn. **57**, 3239 (1988).
[37] K. Nakano, Y. Akahama, Y. Oshishi, and H. Kawamura, Jpn. J. Appl. Phys., Part 1 **39**, 1249 (2000).
[38] H. Kobayashi, R. Kato, A. Kobayashi, S. Moriyama, Y. Nishio, K. Kajita, and W. Sasaki, Synth. Met. **27**, A288 (1988).
[39] K. Kajita, Y. Nishio, T. Takahashi, W. Sasaki, R. Kato, H. Kobayashi, and A. Kobayashi, Solid State Commun. **70**, 1181 (1989).
[40] J. E. Eldridge, Y. Xie, H. H. Wang, J. M. Willimas, A. M. Kini, and J. A. Schlueter, Mol. Cryst. Liq. Cryst. Sci. Technol., Sect. A **284**, 97 (1996).
[41] J. E. Eldridge, C. C. Homes, J. M. Willimas, A. M. Kini, and H. H. Wang, Spectrochim. Acta, Part A **51**, 947 (1995).
[42] M. Maksimuk, K. Yakushi, H. Taniguchi, K. Kanoda, and A. Kawamoto, J. Phys. Soc. Jpn. **70**, 3728 (2001).
[43] Some data points of θ-$(ET)_2I_3$ at 20 K in the low-pressure region are missing because of the disturbance by the huge resonance scattering from I_3^-.
[44] A. Girlando, R. Bozio, and C. Pecile, Phys. Rev. B **26**, 2306 (1982).
[45] I. Tamura, H. Kobayashi, and A. Kobayashi, J. Phys. Chem. Solids **63**, 1255 (2002).
[46] R. Swietlik, D. Schweitzer, and H. J. Keller, Phys. Rev. B **36**, 6881 (1987).
[47] K. Yakushi, H. Kanbara, H. Tajima, H. Kuroda, G. Saito, and T. Mori, Bull. Chem. Soc. Jpn. **60**, 4251 (1987).